Spindle Pole Mechanics Studied in Mitotic Asters: Dynamic Distribution of Spindle Forces through Compliant Linkages

Blake D. Charlebois,[†Δ] Swapna Kollu,[‡Δ] Henry T. Schek 3rd,[§] Duane A. Compton,[‡*] and Alan J. Hunt[†¶*]
[†]Department of Biomedical Engineering, University of Michigan, Ann Arbor, Michigan; [‡]Department of Biochemistry, Dartmouth Medical School, Hanover, New Hampshire; [§]89 North Inc., Burlington, Vermont; and [¶]Center for Ultrafast Optical Science, University of Michigan, Ann Arbor, Michigan

ABSTRACT During cell division, chromosomes must faithfully segregate to maintain genome integrity, and this dynamic mechanical process is driven by the macromolecular machinery of the mitotic spindle. However, little is known about spindle mechanics. For example, spindle microtubules are organized by numerous cross-linking proteins yet the mechanical properties of those cross-links remain unexplored. To examine the mechanical properties of microtubule cross-links we applied optical trapping to mitotic asters that form in mammalian mitotic extracts. These asters are foci of microtubules, motors, and microtubule-associated proteins that reflect many of the functional properties of spindle poles and represent centrosome-independent spindle-pole analogs. We observed bidirectional motor-driven microtubule movements, showing that microtubule linkages within asters are remarkably compliant (mean stiffness 0.025 pN/nm) and mediated by only a handful of cross-links. Depleting the motor Eg5 reduced this stiffness, indicating that Eg5 contributes to the mechanical properties of microtubule asters in a manner consistent with its localization to spindle poles in cells. We propose that compliant linkages among microtubules provide a mechanical architecture capable of accommodating microtubule movements and distributing force among microtubules without loss of pole integrity—a mechanical paradigm that may be important throughout the spindle.

INTRODUCTION

Genome stability requires that chromosomes segregate faithfully during each cell cycle; errors in segregation cause aneuploidy, and can lead to birth defects or contribute to cancer progression. To achieve accurate chromosome segregation, cells assemble a macromolecular ensemble of microtubules, motors, and nonmotor microtubule-associated proteins called the spindle. The spindle is a mechanical apparatus that bears loads and generates directed forces required for appropriate segregation of chromosomes to daughter cells. Multiple forces have been defined within spindles such as polar ejection forces and microtubule depolymerization forces that bring kinetochores to the poles.

Despite our awareness of these spindle forces, there is a dearth of quantitative information about the mechanical properties of spindles. Early micromanipulation experiments yielded predominantly qualitative mechanical data about the spindle (e.g., (1–3)). Subsequent studies have generated quantitative data such as the stall force for anaphase chromosome movement during insect meiosis (4) and the overall distortion of the spindle when subjected to experimentally applied forces (5,6). Optical trapping has been used to measure polar ejection forces in vitro (7) and also to understand the load-bearing mechanical coupling used by kinetochores to harness microtubule depolymerization forces for poleward movement (8,9). Elastic properties of chromosomes and DNA have also been estimated (10,11). Although our limited comprehension of spindle mechanics is aided by quantitative and qualitative studies (12), these few experiments comprise the only mechanical data on spindles.

Spindle poles are sites of convergence of spindle microtubule minus-ends near centrosomes and are the regions of the spindle with the highest density of microtubule-cross-linking (13–15). It has been proposed that poles are key load-bearing structures essential for chromosome movement and generation of euploid cell progeny (16). Despite this importance, no quantitative data exists about the mechanical properties of spindle poles.

Here, we examine the mechanical properties of mitotic asters that recapitulate the properties of spindle poles in a mammalian mitotic cell extract. These asters are composed of microtubules and numerous motor and nonmotor microtubule-associated proteins, and serve as surrogates for mitotic spindle poles. We have previously extensively characterized the biochemical properties of these microtubule asters and have shown that they faithfully recapitulate functional aspects of spindle poles. For mechanical analysis, we have applied optical trapping techniques to this experimental system to study mechanical events at the nanometer scale. With these high-resolution tools, we confirm that asters are steady-state assemblies and show that the linkage of microtubules to the asters is highly compliant. Finally, we combine this approach with

Submitted September 21, 2010, and accepted for publication February 8, 2011.

[Δ]Blake D. Charlebois and Swapna Kollu contributed equally to this work.

*Correspondence: ajhunt@umich.edu or duane.a.compton@dartmouth.edu

Swapna Kollu's present address is Center for Regenerative Medicine, Massachusetts General Hospital, 185 Cambridge St., Boston, MA 02114.

Editor: Douglas Nyle Robinson.

0006-3495/11/04/1756/9 $2.00

doi: 10.1016/j.bpj.2011.02.017

molecular manipulation to explore the contribution of the homotetrameric motor Eg5 to the mechanical properties of spindle poles.

MATERIALS AND METHODS

Cell culture

HeLa cells were maintained in Dulbecco's modified Eagle's medium containing 10% bovine growth serum, 50 IU/mL penicillin, and 50 μg/mL streptomycin. Cells were grown at 37°C in a humidified incubator with a 5% CO_2 atmosphere.

Mitotic aster preparation and assay execution

Mitotic extracts from HeLa cells were prepared according to Gaglio et al. (17). HeLa cells were arrested in mitosis by a double block with 2 mM thymidine followed by nocodazole treatment (10 ng/mL) for 10–12 h. Mitotic cells were collected by shake-off and incubated for 30 min at 37°C with 20 μg/mL cytochalasin B. The cells were then collected by centrifugation at 1500 rpm and washed twice with cold PBS containing 20 μg/mL cytochalasin B. Cells were washed one last time in cold KHMM (78 mM KCl, 50 mM HEPES, 4 mM $MgCl_2$, 1 mM $MnCl_2$, 2 mM EGTA, 1 mM dithiothreitol, pH 7.0) buffer containing 20 μg/mL cytochalasin B, and finally dounce-homogenized (tight pestle) at a concentration of ~3×10^7 cells/mL in KHMM buffer containing 20 μg/mL cytochalasin B, 20 μg/mL phenylmethylsulfonyl fluoride, and 1 μg/mL each of chymostatin, leupeptin, antipain, and pepstatin.

The crude cell extract was then subjected to sedimentation at 20 psi for 20 min at 4°C in an Airfuge (Beckman Coulter, Brea, CA). The supernatant was recovered and supplemented with 2.5 mM ATP (prepared as Mg^{2+} salts in KHMM buffer), 20 μM taxol and 0.075–0.1 mg/mL biotin-tubulin (Cytoskeleton, Denver, CO). For immunodepletions, the supernatant recovered was incubated with antibody-coated agarose beads as described in Gaglio et al. (18) and depletion confirmed by immunoblotting. Where indicated, monastrol was added at this stage at a final concentration of 100 μM. This supernatant was stored on ice up to a maximum of 4 h. To stimulate assembly of mitotic asters, this supernatant mix was incubated at 30°C for 40 min.

After incubation, the extract containing asters was flowed into an experimental chamber with aluminum foil spacers maintaining a chamber depth of ~70 μm, and then sealed with VALAP (a 1:1:1 mixture by mass of Vasoline, lanolin, and paraffin, though we increased the paraffin content by ~8%). Asters were nonspecifically adhered to the coverglass by centrifuging the chamber at 270*g* for 3 min. The VALAP was removed and a solution of KHMM containing 2.5 mM adenine nucleotide, NeutrAvidin-coated beads (prepared as described in Charlebois et al. (19), but with final rinse with and resuspension in KHMM, and with dilution by ~3:100) was flowed in. For monastrol experiments, 100 μM monastrol was also added to this solution. The chamber was then resealed.

With the experimental chamber on the microscope stage (our optical tweezers apparatus is described elsewhere (20,21)), a bead was trapped and brought to microtubules at the aster periphery. Because of the limits of light microscopy, it was not possible to determine unequivocally the exact number of microtubules with which a bead interacted, but the contrast was consistent with one or a few microtubules, and thicker, higher-contrast bundles were avoided. After attachment, an antipoleward force (see Fig. S1 in the Supporting Material; typically 2–4 pN, sufficient to maintain the microtubule under tension but generally not large enough to detach the microtubule) was applied using the force-clamp. Experiments were performed with the top of the bead 1–15 μm below the coverglass, typically 2.5–10 μm, with the bead attached to a microtubule or bundle in the plane of focus.

Tracking movements of microtubules in the aster

Bead and aster focus position were tracked using LabView Vision software (National Instruments, Austin, TX). A rectangular region of interest surrounding the bead or aster focus was chosen and the Vision VI "IMAQ Match Pattern 2" was used to find this pattern in all images for the trace in question. For a given trace, this was repeated with patterns taken from different time points, generally 20–80 s apart, and these resulting image-based traces were averaged. Bead and aster focus positions were then subtracted, yielding changes in bead position relative to the aster focus at ~5 or ~28 Hz. The ~28-Hz traces of aster movement were filtered with a three-point median filter. The uncertainty in bead position relative to the aster focus appears, based on the limited movement in our AMP-PNP data (in which the motors are in rigor, severely restricting microtubule movement; see Fig. 2), to have been small relative to excursions observed in the presence of ATP.

Algorithm identifying excursions of roughly constant velocity

Position versus time traces were analyzed using an algorithm that performs least-squares linear fits to successive time intervals of variable length. Initially a line is fit over a time interval $\tau_{\min} = 2$ s at the beginning of a trace. The algorithm then extends this line forward 1 s. If at least 90% of the residuals (data minus fit) are >10 nm, or if at least 90% of them are <-10 nm, the algorithm rejects the extension and, from the last point of the current (preextension) interval, begins a new fit. Otherwise, the algorithm accepts the first 10% of the data points of the extension, and attempts a new extension.

Computing κ_a from changes in stiffness experienced by the bead

Before attachment to the aster, the stiffness experienced by the bead is due to the known trap stiffness, κ_{trap}. Attachment to an aster increases stiffness to $\kappa_{trap} + \kappa_a$, where κ_a is the effective stiffness experienced by the bead due to its attachment to the aster. Factors contributing to κ_a are the compliance of the bead-microtubule connection (bead rocking) and microtubule-aster focus connection. The former was estimated to be 0.021 pN/nm in a previous study (21). In addition, the sensitivity to conditions under which asters are formed (Fig. 3 *A*), and the consistency with compliances estimated from cross-link breaking events (Fig. 3 *B*), indicate that the compliance is dominated by the microtubule-aster focus connections. By the equipartition theorem, we expect

$$\kappa_{trap} = k_B T / \mathrm{var}\left(x_{pre}\right), \tag{1}$$

$$\kappa_a + \kappa_{trap} = k_B T / \mathrm{var}\left(x_{post}\right), \tag{2}$$

where k_B is Boltzmann's constant, T is the absolute temperature, x_{pre} and x_{post} are the bead position relative to the trap center (x_{bead} in Fig. 1 *C*) before and after attachment, respectively, and var(x) is the variance of x. From Eqs. 1 and 2, we can obtain either of the following:

$$\kappa_a = \kappa_{trap}\left(\frac{\mathrm{var}\left(x_{pre}\right)}{\mathrm{var}\left(x_{post}\right)} - 1\right), \tag{3}$$

$$\kappa_a = k_B T\left(\frac{1}{\mathrm{var}\left(x_{post}\right)} - \frac{1}{\mathrm{var}\left(x_{pre}\right)}\right). \tag{4}$$

Equation 3 has the advantage of being independent of the sensitivity constant used to convert quadrant photodiode voltages to positions, whereas Eq. 4 is independent of the trap stiffness. We used both Eqs. 3 and 4 to

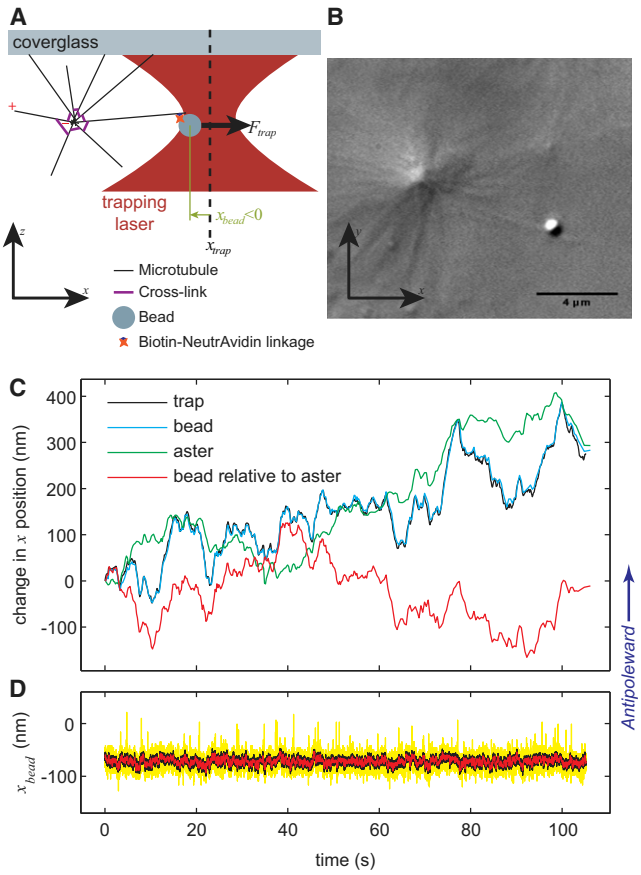

FIGURE 1 Experimental design and example of laser trap analysis of spindle poles. (*A*) Assay schematic: a bead is attached to an aster arm and pulled in the x direction. (*B*) Differential interference contrast image of an aster and attached bead. (*C*) Plot showing position changes versus time. The trap trace is a record of trap movement as controlled by the force clamp routine (10 Hz), whereas the other traces are based on tracking bead and aster movement in images (5 or 30 Hz). The red trace shows bead movement corrected for aster movement. The traces of Fig. 2, Fig. 3 *B*, Fig. S1, and Fig. S2 *A* are corrected in the same manner. Positive direction corresponds to antipoleward direction. (*D*) Plot showing bead position relative to trap center (5 kHz), unfiltered (*yellow*) and low-pass filtered with a cutoff of 100 Hz (*black*) or 10 Hz (*red*) as described in Materials and Methods.

compute each stiffness and averaged these values for each time interval analyzed, yielding Fig. 3 *A* (see later). Values obtained from Eqs. 3 and 4 were similar: the correlation coefficient is $r = 0.94$, and the mean difference is -0.001 pN/nm, SD 0.01 pN/nm.

The expression var(x) was calculated by computing the variance of successive 0.05 s windows (overlapping, with each window beginning 0.01 s after the preceding one) and averaging these variances. T was 307 K.

Computing κ and γ from exponential fits

For the decay toward mechanical equilibrium of a damped harmonic oscillator in low Reynolds number conditions, and under constant force (see free body diagram in Fig. 3 *B*, *inset*), the position, x, as a function of time, t, is

$$x(t) = \frac{F}{\kappa_a} - fe^{-\kappa_a t/\gamma}, \quad (5)$$

where κ_a is as in Fig. 3 *A*, γ is the drag coefficient, F is the applied (force clamp) trap force, and $f \in \mathcal{R}$ is a constant determined by the initial conditions. The values κ_a, γ, and f are fitting parameters. For curve fitting, the data were translated such that the initial time and position were zero. Origin software (OriginLab, Northampton, MA) fit the data to Eq. 5 with initial values $f = 50$ nm, $\kappa_a = 0.03$ pN/nm, and $\gamma = 0.006$ pN/(nm/s). All parameters were restricted to be ≥ 0.

RESULTS AND DISCUSSION

To examine directly the mechanics of microtubule linkages at spindle poles we used cell-free mitotic extracts and optical trapping. Microtubule asters that form in the cell-free system have been extensively characterized, and have been shown to recapitulate accurately spindle-pole organization in cells, including: that they require the biochemical activities of the nonmotor microtubule cross-linking protein NuMA and minus-end-directed motor activity (cytoplasmic dynein, HSET); that they become less tightly focused after depletion of the plus end-directed motor Eg5; that they are sensitive to antagonistic functional relationships between motors with opposite directionality; and that they form in a centrosome-independent manner (17,18,22,23).

Microtubule asters assembled under these conditions lack microtubule polymerization dynamics and poleward microtubule flux at spindle poles. Although the absence of flux is less physiologic, this worked to our advantage in determining the mechanics of microtubule linkages within asters without the confounding influence of microtubule depolymerization at the poles.

For optical trapping, microtubules in the asters were assembled with extract tubulin supplemented with biotinylated tubulin, and the asters were gently centrifuged into contact with a flow-chamber coverglass (Fig. 1 *A*). An optical trap moved a 0.57-μm NeutrAvidin-coated bead into contact with the microtubules at a point far from the aster focus to minimize the number of microtubule attachments (Fig. 1, *A* and *B*). A force-clamp maintained a constant antipoleward force by frequently (10 Hz) repositioning the trap (*black trace* in Fig. 1 *C*) to maintain the displacement of the bead, x_{bead}, relative the to the trap center (Fig. 1 *D*). The positions of the aster focus and bead were tracked using video-enhanced differential interference contrast microscopy (*green* and *cyan traces*, respectively, in Fig. 1 *C*). Changes in bead position relative to the aster focus (*red trace* in Fig. 1 *C*) corresponded to microtubule movement toward or away from the aster focus.

In the presence of ATP, aster microtubules made excursions in both the poleward and antipoleward directions relative to the aster focus (Fig. 1 *C*, Fig. 2 *A*, and Fig. S1). Thus, motors at the pole were capable of generating bidirectional movements but these could have been biased poleward in the presence of dynamic microtubules, resulting in or accommodating poleward flux. Excursions corresponded to intervals of roughly constant velocity, identified by an algorithm (see Materials and Methods) that fit an initial

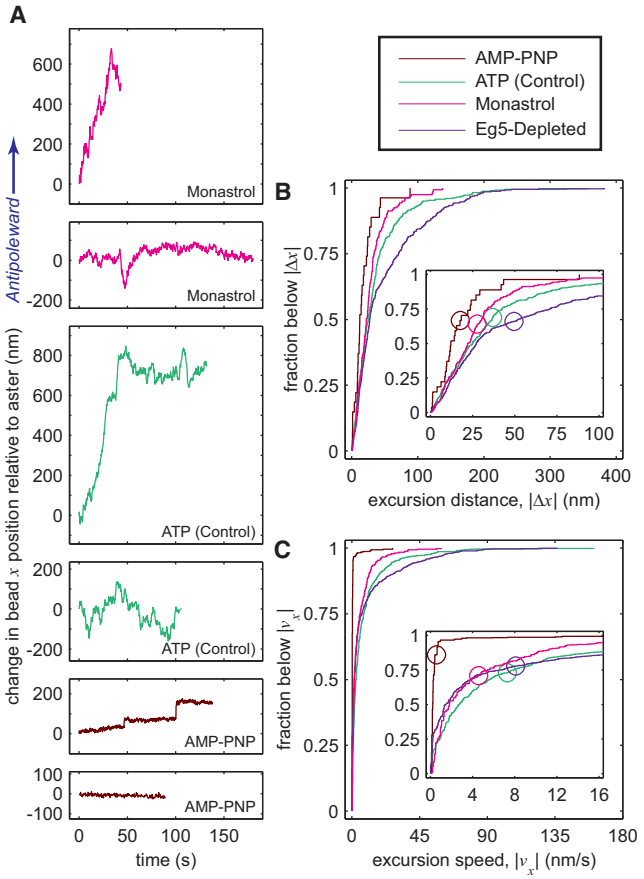

FIGURE 2 Run-lengths and velocities of microtubules anchored to spindle poles. (*A*) Example traces of changes in bead x position relative to the aster versus time (these correspond to the *red trace* of Fig. 1 *C*). Each trace is from a different aster. (*B* and *C*) Analysis of corrected bead movements versus time using an algorithm that fits straight lines to successive time intervals of variable length. Graphs are cumulative distribution function of (*B*) absolute run distance, $|\Delta x|$, and (*C*) time-weighted absolute speed, $|v_x|$. (*Insets*) The same plots zoomed to lower values and with mean absolute values marked with a circle. See also Fig. S1.

window of the position versus time data trace, and projected this fit forward in time until the position data became inconsistent with the constant velocity assumption.

The velocities, v_x, and run-distances, Δx, of these excursions were roughly symmetrically distributed between poleward and antipoleward directions (Fig. S1), although v_x displayed a modest antipoleward bias (roughly 2 nm/s) under the applied forces (typically 2–4 pN; see Table S1). Mean v_x near zero is expected for all conditions that produce asters, as consistent net movement of all microtubules in one direction would result in aster disassembly. Therefore, the range of magnitudes of Δx and of v_x between experimental conditions was compared by their variances (Table S2) and the cumulative distributions of $|\Delta x|$ and $|v_x|$ (Fig. 2, *B* and *C*).

Excursions were highly variable, with some movements persisting for hundreds of nanometers in either direction (Fig. 2 *B* and Fig. S1), consistent with molecular motors taking tens of steps (24,25). The absolute velocity of an excursion, $|v_x|$, was often tens of nm/s (Fig. 2 *C* and Fig. S1). Microtubules sometimes moved hundreds of nm antipoleward before pausing, and could then resume antipoleward excursions or reverse to move poleward (Fig. S1). Because the optical trap applied tension in these experiments, antipoleward movements may have been due to decreased poleward forces, due to disengaging motors for example, rather than active pushing forces. The nonhydrolyzable ATP analog AMP-PNP suppressed poleward and antipoleward microtubule excursions (Fig. 2 *A* and Fig. S1), and this was reflected by significantly lower ($p < 0.05$) variances for v_x and Δx (Table S2). Furthermore, the cumulative distributions of $|\Delta x|$ and $|v_x|$ were shifted toward lower values (Fig. 2, *B* and *C*). These data indicate that bidirectional motion of microtubules in the asters required active microtubule motors.

However, it could be argued that the antipoleward movements observed in the presence of ATP would not occur in the absence of the tension applied by the optical trap. We provide two counterarguments. First, the applied tension (Fig. S1) was usually modest relative to that expected to be developed by a few motors. Second, for motors to cause exclusively poleward movement, plus-directed motors would have to be linked to a static matrix whereas minus-directed motors would have to have their tails attached to moving microtubules while their heads walked on relatively static microtubules. This second argument does not exclude the possibility that there would be no motion in the absence of the optical-trap tension, but a perfectly static aster seems unlikely.

We also note that plus- and minus-end directed motors have been shown to participate in aster organization in this system (18,22,23), and bidirectional movements have been observed in vitro in microtubule gliding assays where motors with opposite directionality act competitively (26), although we detected movement with much higher spatiotemporal resolution and the excursions we observed tended to be much shorter. The ATP-dependent microtubule movements suggest that motors play an important role maintaining the mechanical properties of the aster.

Microtubule movements will strain linkages that hold microtubules to the aster focus. Our assay measures the overall stiffness of the microtubule plus its anchoring by an unknown number of cross-links to the aster. Although the attached bead was located microns from the aster focus, the longitudinal microtubule compliance was negligible compared with the compliances we observed (27–31), so the observed compliance was dominated by compliance at the aster. We measured the stiffness, κ_a, of the bead-microtubule-aster linkages (Fig. 3 *A*, *inset*) by comparing the thermal fluctuations of the bead before and after attachment to an aster microtubule and applying the equipartition theorem.

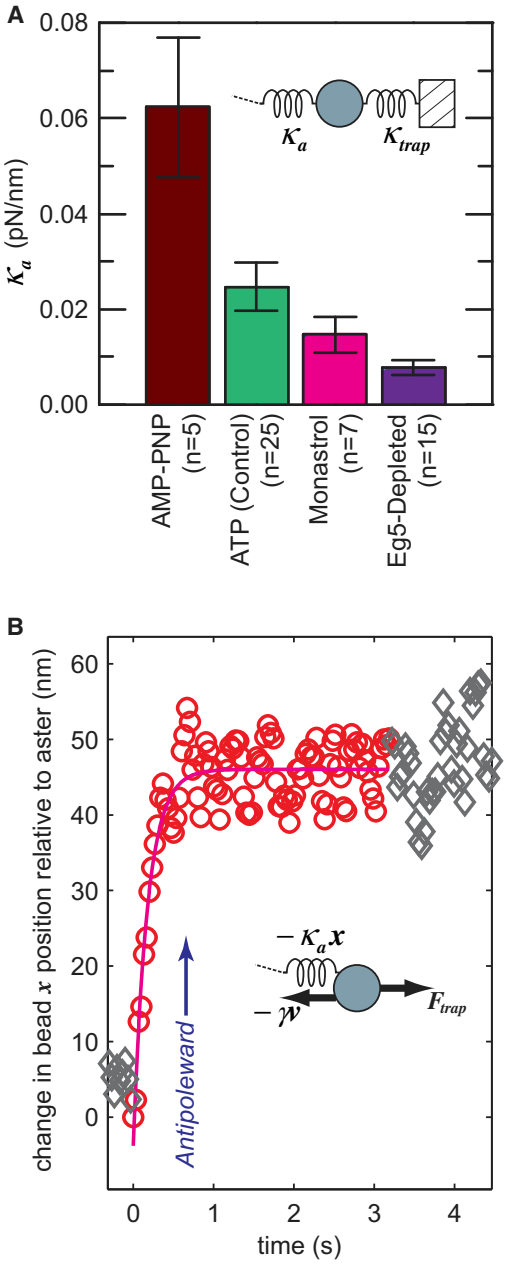

FIGURE 3 Analysis of stiffness of microtubule linkage to spindle poles. (*A*) Values obtained for κ_a under each experimental condition; for a linkage of stiffness κ_a, an applied load F will move the bead a distance F/κ_a. Error bars indicate standard error. The value n represents the number of traces under different experimental conditions including different forces or asters; between three and eight asters were examined for stiffness for each biochemical condition (see Fig. S1). (*Inset*) Physical model from which Eqs. 3 and 4 are derived: the bead is subject to forces from the trap stiffness, κ_{trap}, and the unknown stiffness, κ_a. (*B*) Fit of Eq. 5 to the first exponential jump. The spring force is $-\kappa_a x$ and the drag force $-\gamma v_x$ where κ_a is the stiffness and γ is the drag coefficient. Position data are the corrected bead x positions (see *red trace* of Fig. 1 *C*, and note that aster moved little during this time, as evident in Fig. S2, *B* and *C*). (*Red circles*) Data included in the fit. (*Gray diamonds*) Data points outside this range. (*Magenta line*) The fit. The position and time axes are shifted so the data involved in the fit begin at zero. (*Inset*) Physical model from which Eq. 5 is derived: the bead and aster arm are subject to the force applied by the optical trap in addition to forces equivalent to a Hookean spring of stiffness κ and a force proportional to velocity (dashpot) with drag coefficient γ. See also Fig. S2.

Under control (ATP) conditions, we obtained $\kappa_a = 0.025 \pm 0.005$ pN/nm (mean ± SE; Fig. 3 *A*). This is an order of magnitude less than the rabbit acto-myosin cross-bridge (32) or of several domains of the structural protein titin (33); and it is two orders of magnitude less than a frog extract spindle under gentle compression perpendicular to the metaphase plate (in which there are presumably far more entities acting in parallel against the applied force) (6). However, it is an order of magnitude more than chromosomes (10). When ATP was replaced by AMP-PNP, the stiffness of the linkage increased (Fig. 3 *A*), probably due to more sustained binding of motors to microtubules.

In the presence of AMP-PNP, we observed several abrupt jumps in the position of the bead relative to the aster focus (Fig. 2 *A* and Fig. S2) indicating failures in the mechanical structure. The force applied by our laser trap under these conditions was extremely unlikely to break the NeutrAvidin-biotin linkage between the bead and attached microtubule on the timescale of the experiment (34). Thus, these abrupt jumps most likely represented rupture of a load-bearing cross-link between the microtubule and the aster. These failure events provided a complementary approach to determine the stiffness of the linkage of microtubules to the aster. After each failure, the microtubule relaxed in the direction of the trap force to a new position, which was stable because motor activity was suppressed by AMP-PNP. The exponential form of the jumps was consistent with decay toward mechanical equilibrium of an overdamped harmonic oscillator (i.e., Hookean spring with linear drag) under a constant force, F (Fig. 3 *B*, *inset*), where the low Reynolds number allows mass to be neglected (Eq. 5).

Exponential fits (Fig. 3 *B* and Fig. S2) yielded $\kappa_a = 0.0587 \pm 0.0005$ pN/nm for the first jump and 0.0339 ± 0.0003 pN/nm for the second, consistent with estimates from analysis of thermal motion (Fig. 3 *A*) for the same aster. These exponential jumps, and the decrease in stiffness by roughly half after the first jump, are most directly explained by the loss of microtubule cross-links. As the trace shows no signs of breaks occurring in rapid succession, and because it is unlikely that several cross-links would break at the beginning of the jump simultaneously (within roughly 0.1 s of each other), it is reasonable to expect that each event corresponded to failure of a single microtubule cross-link. Assuming the cross-links had similar compliances, the 43% stiffness decrease after the second break suggests the breaking cross-link was 1 among 2–3, in which case there were 3–4 cross-links at the beginning of the trace. Although these estimates are from fortuitous observations of cross-link breaking, the consistency of the stiffness with other asters (Fig. 3 *B*) suggests they are not atypical.

Exponential fits to each jump (Fig. 3 *B* and Fig. S2) yielded drag coefficients, γ, of 10.4 $\pm$ 0.9 pN·s/μm for the first jump and 7.4 $\pm$ 0.5 pN·s/μm for the second. These values are three orders-of-magnitude larger than expected from viscous drag on the microtubule and bead (see Discussion A in the Supporting Material), presumably because relaxation also involved shifting of microtubules attached to the microtubule under consideration, with possible contributions from friction between moving components of the aster. High drag is likely to be physiologically important, as it will slow the movement of a microtubule that detaches under tension, and thereby allow more time for motors and cross-linkers to make new attachments. However, the drag was not so high as to overload mitotic motors; at typical ~10 nm/s speeds of microtubule flux (35), the drag is well below the pN forces that are commonly developed by individual motor proteins.

The kinesin-5 motor Eg5, in addition to sliding antiparallel microtubules to promote spindle bipolarity, localizes strongly to spindle poles (36) where it is presumed to cross-link microtubules. It is required for tight focusing of microtubules into asters in this cell-free system and in cells and other model systems (18,36). To examine the mechanical role of Eg5 within these microtubule asters, we inhibited its activity by immunodepletion or with the small molecule inhibitor monastrol. With either perturbation, there was no detectable change in mean microtubule excursion velocity or distance compared to controls (Fig. 2, *B* and *C*, and Table S2). However, the variance of excursion velocity and distance was higher in Eg5-depleted asters (Table S2), indicating that the microtubules exhibited a greater range of speed and displacement, in both directions, compared to control asters. This was likely a consequence of greater mechanical compliance, as analysis of thermal motion suggests control asters were stiffer than those formed under Eg5-depleted conditions (Fig. 3 *A*, Table S3 and Table S4).

The stiffness of monastrol-treated asters was less than controls and more than Eg5-depleted asters, though not reaching statistical significance from either (Fig. 3 *A*, Table S3 and Table S4). This is consistent with the observation that monastrol has little effect on Eg5's binding affinity to microtubules (37,38), and suggests that cross-linking by Eg5 tetramers in the presence of monastrol contributes to aster stiffness even though motor activity is inhibited. Although monastrol does not affect Eg5's binding affinity, it still inhibits Eg5's catalytic activity, and thus may still impact the compliance of the asters. This is in agreement with our observation that the compliance of asters is slightly increased in the presence of monastrol, reflecting the contribution of Eg5's motor activity to the aster core's compliance. Taken together, our Eg5-perturbation results suggest that Eg5 imparts stiffness to poles where it cross-links parallel microtubules, which is consistent with the report that bipolar spindles formed in frog egg extracts lacking Eg5 are fragile (39).

Microtubules in the mitotic spindle converge as they approach the centrosomes at the spindle poles. Pole-focusing components such as motor (cytoplasmic dynein, Eg5, and HSET) and nonmotor (NuMA) proteins cross-link and focus microtubule minus-ends at the poles. Given their proximity, centrosomes may contribute to the mechanical properties of the spindle pole. The studies described here examine the mechanical properties of the acentrosomal asters assembled from cell-free extracts, and are thus most relevant for understanding the role of these cross-linkers. We found that connections between microtubules and the aster focus were very compliant. The source of this compliance is at least partially motor-based as inhibition of motor activity by AMP-PNP reduces the compliance. Nonmotor proteins such as NuMA that can oligomerize via its large coiled-coil region (40) to provide a polymeric matrix may also be contributing to compliance.

We propose that this mechanical property is critical to preserve spindle architecture as individual microtubules experience poleward and antipoleward displacements. Highly compliant microtubule linkages increase the load any individual microtubule can bear by distributing forces among microtubules and motors, similar to a truss (Fig. 4 *A*). However, compliance must be low enough that significant force redistribution occurs before a microtubule under tension is pulled out of the pole. This is consistent with our compliance data showing that ~2 pN would be transmitted after ~80-nm movement, which is small compared to the micron-scale poles. On the other hand, compliance must not be too low, because rigid cross-links will resist relative sliding of adjacent microtubules, which is required for processes such as poleward flux and for changes in the positions of chromosomes (Fig. 4, *B* and *C*). The compliances we measured would allow a motor to take at least 10 steps before encountering a load that would induce, for instance, Eg5 detachment (24,41). Thus, to support more extended movements as seen during poleward flux, cross-links must periodically rearrange to relieve strain. If the compliance were lower such rearrangements would have to occur more frequently, thus diminishing their effectiveness transferring force between microtubules.

A simple model (see Discussion B in the Supporting Material) suggests an order-of-magnitude decrease in compliance would diminish the effectiveness of force transfer to the point where microtubules would be frequently lost from the pole if there was not a compensating shift in cross-link dynamics (i.e., an increase in the number of cross-links or in the rate that the new cross-links form). Conversely, an order-of-magnitude increase in the compliance would result in severe distortions in the spindle structure that are not observed in vitro. Furthermore, rigid microtubule cross-linking would fix the angles between microtubules, so that one motor walking along a microtubule would force another motor to disengage (Fig. 4 *C*, as opposed to Fig. 4 *B*).

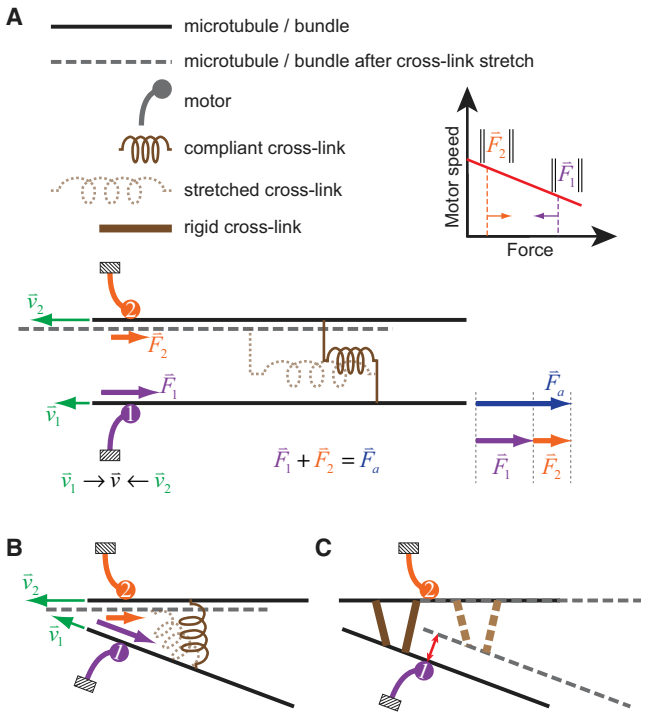

FIGURE 4 Model explaining the effect of cross-link stiffness on force distribution at spindle poles. (*A*) Force distribution and velocity coordination for parallel microtubules. When $\vec{F}_a$ is applied, motor 1 (*purple*) must sustain initially $\vec{F}_1 \approx \vec{F}_a$, slowing the motor as determined by its force-velocity relationship. The unloaded microtubule does not change speed, but as the cross-link stretches and therefore transmits more force, some of $\vec{F}_a$ is distributed via the cross-link to motor 2 as $\vec{F}_2$, which relieves some of the load on motor 1: $\|\vec{F}_1\| < \|\vec{F}_a\|$. This slows motor 2 and speeds motor 1 so that the two approach roughly the same speed. Motors and compliant cross-links are shown as distinct entities for simple depiction of force transfer; the concept is not changed if motors also act as cross-links. (*B*) Nonparallel microtubules. As in the parallel case, force is transmitted via the cross-link. The component of force transmitted parallel to the microtubule increases if the angles between the cross-link and microtubules decrease, which occurs with increasing load. Note that for clarity the angle is greater than would typically be observed for adjacent microtubules. However, the concepts depicted here and in panel *C* also apply for indirectly cross-linked microtubules, which are found at all angles across the spindle pole. (*C*) Rigidly cross-linked microtubules. With sufficient rigid cross-linking, the relative positions of all microtubules are fixed. Microtubules move with the same speed and direction, and geometric constraints prevent motors from walking along microtubules while remaining fixed. The structure cannot rearrange to accommodate mitotic phenomena such as flux unless the cross-links are transient relative to the rate at which motors move, in which case they transmit less force and therefore distribute a smaller amount of the load from one microtubule to another. (See also Fig. S3.)

Matos et al. (42) have recently proposed that poleward flux-associated slipping of microtubule attachments at kinetochores combined with a visco-elastic coupling of microtubules to the poles comprises a system that can equilibrate tensions across chromosome kinetochores, thus coordinating their movement at the onset of anaphase. Our findings roughly support the model of Matos et al., but suggest that an effect similar to the drag force mediated in their model by passive dashpot elements in series with compliant elements may be mediated in part by ATP-hydrolyzing motors.

The implication of force transmission by compliant cross-links is that a load on any particular microtubule or microtubule bundle is not borne entirely by the motors directly interacting with that microtubule (Fig. 4 *A*). A corollary is that loads are distributed among motors such that the speeds that microtubules move is relatively coordinated even if their pole-distal ends are attached to different structures and subject to different loads (Fig. 4 *A*). For example, a tension opposing poleward movement of a microtubule will slow not only that microtubule, but also the poleward movement of its neighbors. Likewise, the maximum force that can be sustained by one microtubule or bundle in a half-spindle is potentially augmented by motors on neighboring microtubules, with the amount of force transfer diminishing for microtubules more distantly separated in the spindle.

In this context, earlier estimates of spindle forces should be reconsidered. A maximum force of 750 pN (±50%) was estimated by Nicklas (4) using a flexible glass microneedle to stall the poleward movement of an individual chromosome in anaphase in *Melanoplus* spermatocytes, which is 10,000 times that required to overcome viscous drag. Microtubule flux is the dominant mechanism for poleward movement of chromosomes during anaphase in *Melanoplus* spermatocytes (43), so the slowing of chromosomes by an opposing load is most simply explained by slowing poleward flux. Because the forces on spindle microtubules will be distributed among the force generators responsible for flux, the numbers obtained by Nicklas (4) may reflect an integrated force, perhaps reflecting the force that the half-spindle produces to move multiple chromosomes.

CONCLUSION

These findings describe microtubule attachments to asters in a mammalian mitotic extract as compliant and dynamic, with individual microtubules anchored by a small number of motors and nonmotors to maintain the overall structure while accommodating and driving microtubule movements. Such a structural framework is consistent with recent work from Gatlin et al. (13) who found that although poles are densely cross-linked structures, they are compliant enough to let a spearing microneedle pass through them.

A similar theme is suggested at the spindle midzone in the proposal in Subramanian et al. (44) that the protein PRC1 uses dynamic, compliant cross-linking of microtubules at the spindle midzone to balance structural rigidity with the flexibility needed to allow microtubule sliding by kinesin-5 motors. Thus, we envision that this dynamic, compliant mechanical architecture may not be restricted to the polar region of spindles but is used throughout spindles to distribute forces needed for steady-state assembly and

chromosome movement. We anticipate that future studies of the mechanics of spindle components, including poles containing centrosomes, may reveal dynamic compliant linkages as a central theme within the mitotic spindle, which must maintain mechanical integrity without impeding pervasive dynamic movements.

SUPPORTING MATERIAL

Two discussion sections, eight equations, three tables, and three figures are available at http://www.biophysj.org/biophysj/supplemental/S0006-3495(11)00234-7.

We thank J. Damon Hoff for fruitful discussions and for a critical reading of an early typescript.

This work was supported by grants from the National Institutes of Health to D.A.C. (No. GM51542) and A.J.H. (No. GM076177).

REFERENCES

1. Nicklas, R. B., and C. A. Staehly. 1967. Chromosome micromanipulation. I. The mechanics of chromosome attachment to the spindle. *Chromosoma.* 21:1–16.
2. Begg, D. A., and G. W. Ellis. 1979. Micromanipulation studies of chromosome movement. I. Chromosome-spindle attachment and the mechanical properties of chromosomal spindle fibers. *J. Cell Biol.* 82:528–541.
3. Begg, D. A., and G. W. Ellis. 1979. Micromanipulation studies of chromosome movement. II. Birefringent chromosomal fibers and the mechanical attachment of chromosomes to the spindle. *J. Cell Biol.* 82:542–554.
4. Nicklas, R. B. 1983. Measurements of the force produced by the mitotic spindle in anaphase. *J. Cell Biol.* 97:542–548.
5. Dumont, S., and T. J. Mitchison. 2009. Compression regulates mitotic spindle length by a mechanochemical switch at the poles. *Curr. Biol.* 19:1086–1095.
6. Itabashi, T., J. Takagi, …, S. Ishiwata. 2009. Probing the mechanical architecture of the vertebrate meiotic spindle. *Nat. Methods.* 6: 167–172.
7. Brouhard, G. J., and A. J. Hunt. 2005. Microtubule movements on the arms of mitotic chromosomes: polar ejection forces quantified in vitro. *Proc. Natl. Acad. Sci. USA.* 102:13903–13908.
8. Hunt, A. J., and J. R. McIntosh. 1998. The dynamic behavior of individual microtubules associated with chromosomes in vitro. *Mol. Biol. Cell.* 9:2857–2871.
9. Powers, A. F., A. D. Franck, …, C. L. Asbury. 2009. The Ndc80 kinetochore complex forms load-bearing attachments to dynamic microtubule tips via biased diffusion. *Cell.* 136:865–875.
10. Poirier, M. G., S. Eroglu, and J. F. Marko. 2002. The bending rigidity of mitotic chromosomes. *Mol. Biol. Cell.* 13:2170–2179.
11. Bloom, K. S. 2008. Beyond the code: the mechanical properties of DNA as they relate to mitosis. *Chromosoma.* 117:103–110.
12. Mogilner, A., and E. Craig. 2010. Towards a quantitative understanding of mitotic spindle assembly and mechanics. *J. Cell Sci.* 123:3435–3445.
13. Gatlin, J. C., A. Matov, …, E. D. Salmon. 2010. Directly probing the mechanical properties of the spindle and its matrix. *J. Cell Biol.* 188:481–489.
14. Mastronarde, D. N., K. L. McDonald, …, J. R. McIntosh. 1993. Interpolar spindle microtubules in PTK cells. *J. Cell Biol.* 123:1475–1489.
15. Nicklas, R. B., D. F. Kubai, and T. S. Hays. 1982. Spindle microtubules and their mechanical associations after micromanipulation in anaphase. *J. Cell Biol.* 95:91–104.
16. Gordon, M. B., L. Howard, and D. A. Compton. 2001. Chromosome movement in mitosis requires microtubule anchorage at spindle poles. *J. Cell Biol.* 152:425–434.
17. Gaglio, T., A. Saredi, and D. A. Compton. 1995. NuMA is required for the organization of microtubules into aster-like mitotic arrays. *J. Cell Biol.* 131:693–708.
18. Gaglio, T., A. Saredi, …, D. A. Compton. 1996. Opposing motor activities are required for the organization of the mammalian mitotic spindle pole. *J. Cell Biol.* 135:399–414.
19. Charlebois, B. D., H. T. Schek, and A. J. Hunt. 2010. Nanometer-resolution microtubule polymerization assays using optical tweezers and microfabricated barriers. *In* Microtubules, in Vitro. Methods in Cell Biology, *Vol. 95*. J. J. Correia, editor. Elsevier, Amsterdam, The Netherlands. 203–215.
20. Brouhard, G. J., H. T. Schek, 3rd, and A. J. Hunt. 2003. Advanced optical tweezers for the study of cellular and molecular biomechanics. *IEEE Trans. Biomed. Eng.* 50:121–125.
21. Schek, 3rd, H. T., M. K. Gardner, …, A. J. Hunt. 2007. Microtubule assembly dynamics at the nanoscale. *Curr. Biol.* 17:1445–1455.
22. Gaglio, T., M. A. Dionne, and D. A. Compton. 1997. Mitotic spindle poles are organized by structural and motor proteins in addition to centrosomes. *J. Cell Biol.* 138:1055–1066.
23. Mountain, V., C. Simerly, …, D. A. Compton. 1999. The kinesin-related protein, HSET, opposes the activity of Eg5 and cross-links microtubules in the mammalian mitotic spindle. *J. Cell Biol.* 147:351–366.
24. Valentine, M. T., P. M. Fordyce, …, S. M. Block. 2006. Individual dimers of the mitotic kinesin motor Eg5 step processively and support substantial loads in vitro. *Nat. Cell Biol.* 8:470–476.
25. Toba, S., T. M. Watanabe, …, H. Higuchi. 2006. Overlapping hand-over-hand mechanism of single molecular motility of cytoplasmic dynein. *Proc. Natl. Acad. Sci. USA.* 103:5741–5745.
26. Tao, L., A. Mogilner, …, J. M. Scholey. 2006. A homotetrameric kinesin-5, KLP61F, bundles microtubules and antagonizes Ncd in motility assays. *Curr. Biol.* 16:2293–2302.
27. Gittes, F., B. Mickey, …, J. Howard. 1993. Flexural rigidity of microtubules and actin filaments measured from thermal fluctuations in shape. *J. Cell Biol.* 120:923–934.
28. Venier, P., A. C. Maggs, …, D. Pantaloni. 1994. Analysis of microtubule rigidity using hydrodynamic flow and thermal fluctuations. *J. Biol. Chem.* 269:13353–13360.
29. Mickey, B., and J. Howard. 1995. Rigidity of microtubules is increased by stabilizing agents. *J. Cell Biol.* 130:909–917.
30. Felgner, H., R. Frank, and M. Schliwa. 1996. Flexural rigidity of microtubules measured with the use of optical tweezers. *J. Cell Sci.* 109:509–516.
31. Tuszyński, J. A., T. Luchko, …, J. M. Dixon. 2005. Anisotropic elastic properties of microtubules. *Eur. Phys. J. E Soft Matter.* 17:29–35.
32. Veigel, C., M. L. Bartoo, …, J. E. Molloy. 1998. The stiffness of rabbit skeletal actomyosin cross-bridges determined with an optical tweezers transducer. *Biophys. J.* 75:1424–1438.
33. Rief, M., M. Gautel, …, H. E. Gaub. 1997. Reversible unfolding of individual titin immunoglobulin domains by AFM. *Science.* 276: 1109–1112.
34. Yuan, C. B., A. Chen, …, V. T. Moy. 2000. Energy landscape of streptavidin-biotin complexes measured by atomic force microscopy. *Biochemistry.* 39:10219–10223.
35. Cameron, L. A., G. Yang, …, E. D. Salmon. 2006. Kinesin 5-independent poleward flux of kinetochore microtubules in PtK1 cells. *J. Cell Biol.* 173:173–179.
36. Sawin, K. E., K. LeGuellec, …, T. J. Mitchison. 1992. Mitotic spindle organization by a plus-end-directed microtubule motor. *Nature.* 359:540–543.
37. Cochran, J. C., J. E. Gatial, 3rd, …, S. P. Gilbert. 2005. Monastrol inhibition of the mitotic kinesin Eg5. *J. Biol. Chem.* 280:12658–12667.

38. Kwok, B. H., L. C. Kapitein, …, T. M. Kapoor. 2006. Allosteric inhibition of kinesin-5 modulates its processive directional motility. *Nat. Chem. Biol.* 2:480–485.

39. Mitchison, T. J., P. Maddox, …, T. M. Kapoor. 2005. Roles of polymerization dynamics, opposed motors, and a tensile element in governing the length of *Xenopus* extract meiotic spindles. *Mol. Biol. Cell.* 16:3064–3076.

40. Saredi, A., L. Howard, and D. A. Compton. 1996. NuMA assembles into an extensive filamentous structure when expressed in the cell cytoplasm. *J. Cell Sci.* 109:619–630.

41. Korneev, M. J., S. Lakämper, and C. F. Schmidt. 2007. Load-dependent release limits the processive stepping of the tetrameric Eg5 motor. *Eur. Biophys. J.* 36:675–681.

42. Matos, I., A. J. Pereira, …, H. Maiato. 2009. Synchronizing chromosome segregation by flux-dependent force equalization at kinetochores. *J. Cell Biol.* 186:11–26.

43. Chen, W., and D. H. Zhang. 2004. Kinetochore fiber dynamics outside the context of the spindle during anaphase. *Nat. Cell Biol.* 6:227–231.

44. Subramanian, R., E. M. Wilson-Kubalek, …, T. M. Kapoor. 2010. Insights into antiparallel microtubule crosslinking by PRC1, a conserved nonmotor microtubule binding protein. *Cell.* 142:433–443.